

8-1999

Cell/Dendrite Distribution in Directionally Solidified Hypoeutectic Pb-Sb Alloys

S. P. O'Dell
Cleveland State University

G. L. Ding
Cleveland State University

Surendra N. Tewari
Cleveland State University

Follow this and additional works at: https://engagedscholarship.csuohio.edu/encbe_facpub

 Part of the [Materials Science and Engineering Commons](#)

How does access to this work benefit you? Let us know!

Original Citation

O'Dell, S.P., Ding, G.L., & Tewari, S.N. (1999). Cell/Dendrite Distribution in Directionally Solidified Hypoeutectic Pb-Sb Alloys. *Metallurgical and Materials Transactions A: Physical Metallurgy and Materials Science* 30, 2159-2165.

Repository Citation

O'Dell, S. P.; Ding, G. L.; and Tewari, Surendra N., "Cell/Dendrite Distribution in Directionally Solidified Hypoeutectic Pb-Sb Alloys" (1999). *Chemical & Biomedical Engineering Faculty Publications*. 4.
https://engagedscholarship.csuohio.edu/encbe_facpub/4

This Article is brought to you for free and open access by the Chemical & Biomedical Engineering Department at EngagedScholarship@CSU. It has been accepted for inclusion in Chemical & Biomedical Engineering Faculty Publications by an authorized administrator of EngagedScholarship@CSU. For more information, please contact library.es@csuohio.edu.

Cell/Dendrite Distribution in Directionally Solidified Hypoeutectic Pb-Sb Alloys

S.P. O'DELL, G.L. DING, and S.N. TEWARI

The alloys Pb-2.2 wt pct Sb and Pb-5.8 wt pct Sb were directionally solidified with three different thermal gradients of 40, 86, and 140 K cm⁻¹ at growth rates ranging from 0.6 to 30 μm s⁻¹. A Gaussian peak amplitude analysis of the cell/dendrite spacing distribution shows a distinct peak corresponding to the nearest neighbors. The peaks corresponding to the second and the third nearest neighbor spacings are also brought out by this technique. The ratios of the second to the first nearest neighbor spacings and that of the third to the first neighbor spacings are 1.85 ± 0.11 and 2.70 ± 0.25, respectively. This indicates that the cells and dendrites both have a hexagonal distribution with a significant amount of superimposed noise. This is also confirmed by the frequency distribution of their number of nearest neighbors (coordination number).

I. INTRODUCTION

PRIMARY dendrites and their distribution influence the mechanical properties of cast components. Their processing-parameter dependence has therefore been extensively investigated. Theoretical analyses have generally assumed a two-dimensional (2-D) axisymmetric distribution of dendrites.^[1,2] Only recently has three-dimensional (3-D) analysis of dendrites been attempted by phase-field methods.^[3,4] An extensive body of literature exists on the dependence of the average primary spacing on the composition, growth speed, and thermal gradients for both the cellular and dendritic morphologies. Primary dendrite spacing has generally been measured as $(A)^{0.5}/N$, where N is the number of dendrites in a given area A on a cross section that is transverse to the growth direction. This technique inherently assumes a square distribution of dendrites on the transverse cross section. A square distribution of dendrites has been assumed for modeling mushy-zone permeability.^[5] A rectangular distribution has been assumed for examining the interaction among neighboring dendrites.^[6] Each primary dendrite does have a fourfold symmetry in terms of its side-branch formation, but the distribution of many dendrites with respect to each other on the transverse section may not be square or rectangular. No detailed statistical examination of the primary dendrite distribution has been reported. There is only one such study reported in the literature, and that is for the cellular array in directionally solidifying Pb-Tl alloy.^[7] Here, the cellular distribution was examined using a Wigner-Seitz construction of cell boundaries followed by minimum spanning tree analysis. This analysis demonstrated that the cells have a hexagonal distribution with random superimposed noise.

Theoretical analyses of the mechanisms responsible for determining the range of primary spacings observed during directional solidification at a given speed, taking into account the recently discovered history dependence of the average

primary spacing,^[8,9] would require a detailed statistical analysis of the distribution of the nearest and higher-order primary dendrite spacings. The purpose of this research was to compare the cells and dendrites in directionally solidified metallic alloys for statistical distribution of nearest and higher-order neighbor spacings, and also to compare them for the frequency distribution of their coordination numbers (*i.e.*, their number of nearest neighbors)

During directional solidification of metallic alloys, with melt on top and solid below, the thermal profile is expected to cause stability against convection. However, the solutal profile in the mushy zone and in the overlying melt immediately ahead of the dendritic array would be expected to cause stability only if the solute enrichment increases the melt density (for example, hypoeutectic Al-Cu alloys). In binary alloys where the solute enrichment decreases the melt density (*e.g.*, hypoeutectic Pb-Sn alloys), significant convection is expected. The logical choice for our study would, therefore, have been hypoeutectic Al-Cu alloys. However, these alloys are prone to "steeping," clustering of dendrites on the sample cross section, which produces a very nonuniform transverse microstructure.^[10] Although the solutally unstable alloys are susceptible to convection, a uniform primary dendrite distribution across the entire sample cross section is generally obtained,^[11] unless the growth conditions are pushed into the domain of "freckle" or "chimney" formation in the mushy zone.^[12] Therefore, for this study, solutally unstable growth conditions were selected, using Pb-2.2 wt pct Sb and Pb-5.8 wt pct Sb alloys. The solute content of the first alloy is less than the maximum solubility limit of antimony in lead (a freezing range of 61 K with about 9 pct eutectic liquid) and that of the second alloy is more than the solubility limit (a freezing range of 37 K with about 38 pct eutectic liquid). Hence, the second alloy was expected to have a more permeable mushy zone and more thermosolutal convection.

II. EXPERIMENTAL PROCEDURES

The roughly 24- to 30-cm-long Pb-2.2 wt pct Sb and Pb-5.8 wt pct Sb feedstock samples were obtained by induction melting a charge (lead 99.99 pct purity and antimony 99.999 pct purity) under an ultra-high-purity argon atmosphere in

S.P. O'DELL, Undergraduate Student, G.L. DING, Research Associate, and S.N. TEWARI, Professor, are with the Chemical Engineering Department, Cleveland State University, Cleveland, OH 44115.

Manuscript submitted October 8, 1998.

MACROSEGREGATION ALONG THE DS LENGTH

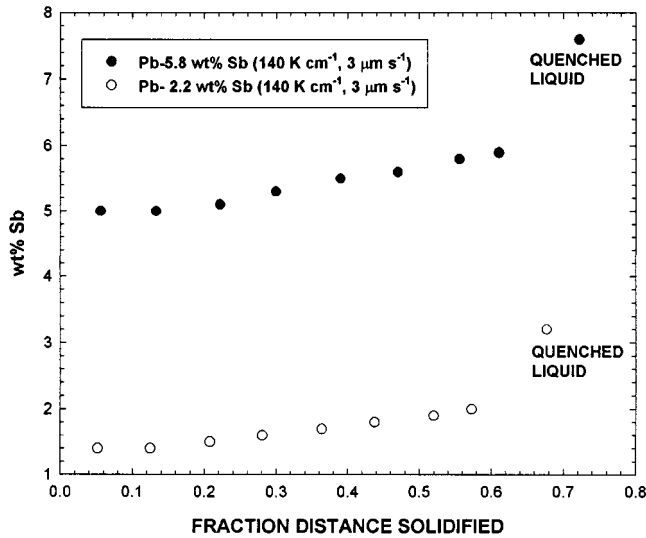


Fig. 1—Axial variation in antimony content due to macrosegregation in directionally solidified samples of Pb-2.2 wt pct Sb and Pb-5.8 wt pct Sb, grown at $V = 3 \mu\text{m s}^{-1}$ and $G = 140 \text{ K cm}^{-1}$.

a graphite crucible and then pushing the melt into evacuated quartz tubes (0.6-cm i.d.) with the aid of argon pressure. These cast rods were then placed in quartz ampoules (0.7-cm i.d., 61-cm long), which were sealed at the bottom. Directional solidification was carried out in a flowing argon atmosphere by pulling the ampoule from the hot zone of the furnace at speeds ranging from 0.8 to $30 \mu\text{m s}^{-1}$. The thermal profile during directional solidification was recorded by Chromel–Alumel thermocouples (0.01-cm diameter) placed in 0.06-cm o.d. quartz capillaries inside the melt. Directional solidification was carried out under steady-state thermal profiles, as evidenced by the identical thermal profiles recorded by three thermocouples that were placed 2 cm apart along the sample axis. After about 7 cm of directional solidification, the quartz ampoule was quickly withdrawn from the furnace and quenched by spraying water. Three different thermal gradients, 40, 86, and 140 K cm^{-1} , were used in the present investigation. Microstructures were observed by standard optical metallography techniques on the longitudinal (parallel to the growth direction) and transverse sections using an etchant made up of 70 mL acetic acid and 30 mL H_2O_2 (30 pct).

III. RESULTS

A. Macrosegregation Due to Convection

Figure 1 shows typical antimony content along the directionally solidified length of the Pb-2.2 wt pct Sb and Pb-5.8 wt pct Sb samples grown at $3 \mu\text{m s}^{-1}$ and 140 K cm^{-1} . The composition of the quenched liquid portion of the samples are indicated as “quenched liquid.” In comparison, the composition variation along the length of as-cast feedstock samples was typically within ± 0.15 wt pct Sb. Longitudinal macrosegregation in the directionally solidified samples is evidence of convection and mixing of the interdendritic mushy-zone liquid with the overlying melt.

B. Distribution of Nearest and Higher-Order Intercellular and Interdendritic Spacings

Figures 2(a) and (b), respectively, show typical quenched microstructure for cellular and dendritic morphologies in directionally solidified Pb-2.2 wt pct Sb alloy. The longitudinal sections show that the cells and dendrites were well aligned parallel to the growth direction, as indicated by the longitudinal views. Distribution of cells and dendrites on the transverse section was also uniform, as typically shown in the transverse views.

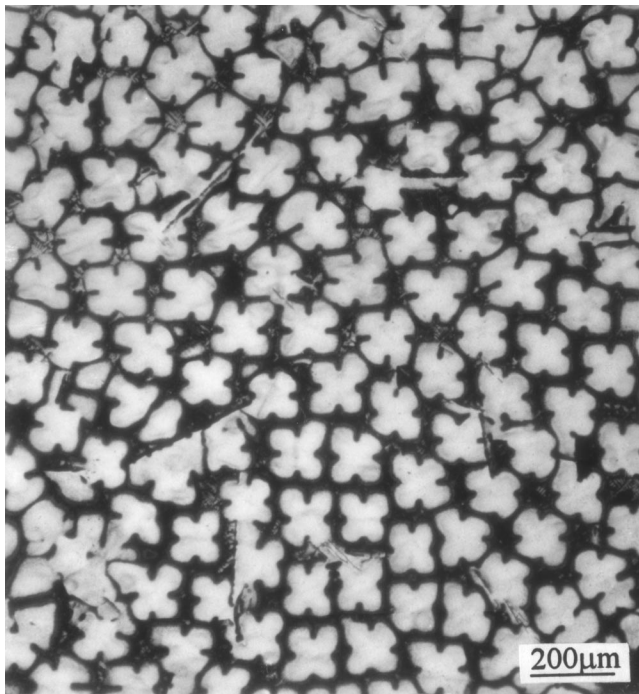
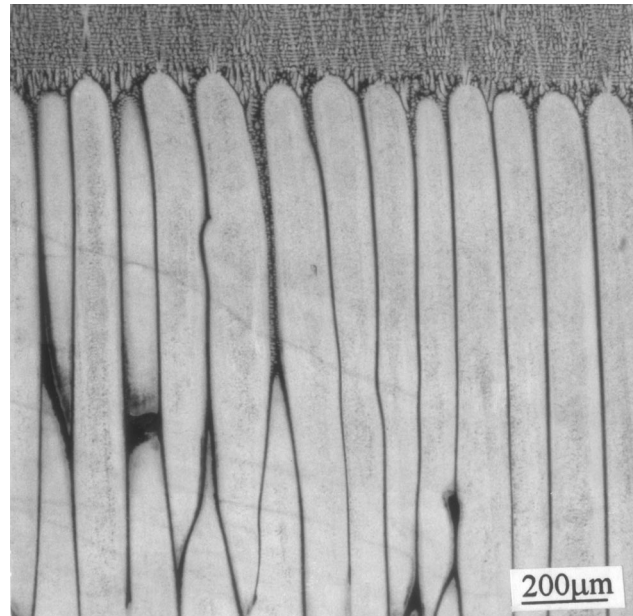
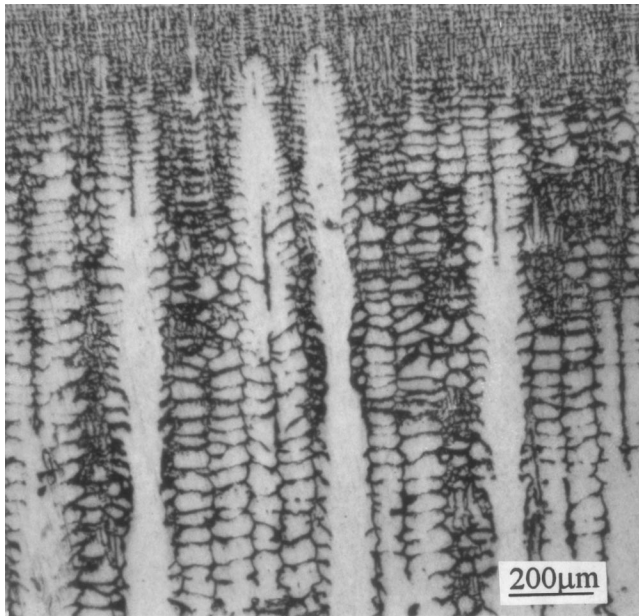
Figures 3(a) and (b), respectively, give typical distributions of nearest and higher-order primary spacings for cells and dendrites. The spacing data in this figure correspond to the distance between the centroids of the cells or dendrites. There is a very distinct peak corresponding to the nearest neighbors for both the cellular and dendritic morphologies. The second nearest neighbor peak is less distinct. Higher-order spacing peaks are masked by the large disorder in the spatial distribution of dendrites and cells. In order to deconvolute the hidden peaks, the spacing distribution data were analyzed by PEAKFIT* 4.06 software, using Gaussian

*PEAKFIT is a trademark of SPSS Inc., Chicago, IL.

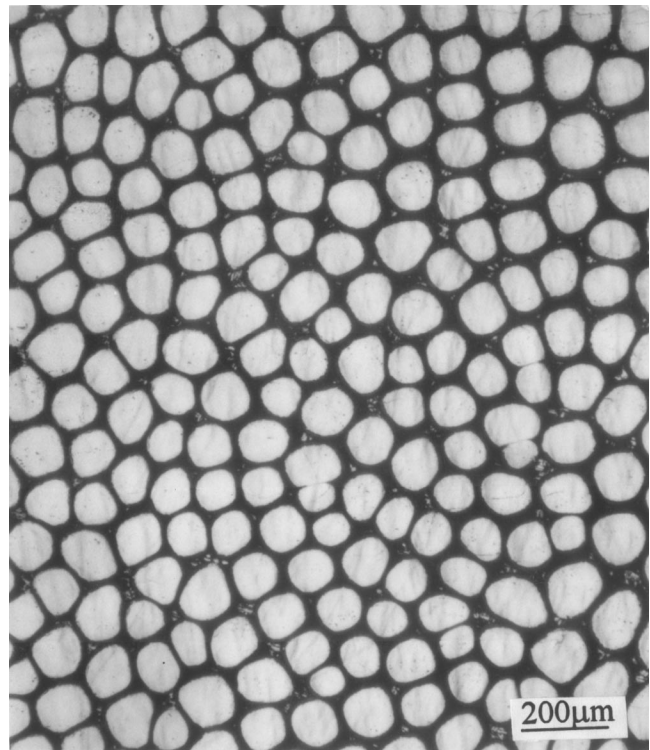
amplitude analysis with variable peak width following subtraction of the linear background. The spacing distribution was smoothed using a utility called Automated FFT Smoothing in the PEAKFIT 4.06 software. The spacing distribution data smoothed in this manner are shown in Figures 3(a) and (b). The smoothed data are then fitted to Gaussian amplitude using another utility called Automatic Peak Detection & Fitting, Method III in the PEAKFIT software. This utility automatically detects peaks and fits the data to a Gaussian amplitude by de-convolution. The obtained typical results for the cellular and dendritic microstructures shown in Figures 2(a) and (b) are given in Figures 4(a) and (b), respectively. For each Gaussian peak, the frequency F is given as $F = A_0 \exp[-0.5((X - A_1)/A_2)^2]$, where X is the spacing, A_0 is the peak amplitude, A_1 the peak center, and A_2 the peak width parameter (standard deviation). The fitting coefficients of determination (r^2) to Gaussian amplitude are 0.98 and 0.96 for the two cases shown in Figures 4(a) and (b), respectively, indicating a good fit to the Gaussian distribution. Table I presents the similarly obtained results for the Pb-2.2 wt pct Sb alloy grown at various speeds under a thermal gradient of 86 K cm^{-1} . The three parameters, A_0 , A_1 , and A_2 , are listed, respectively, for the three peaks. Column 5 lists the various r^2 values. High values of r^2 in Table I indicate that the spacing distribution data for both the cells and dendrites can be described by Gaussian peaks corresponding to the first, second, and the third nearest neighbor spacings. Table I also lists the ratio of the width parameter (A_2) and the peak center (A_1) for the nearest neighbor peaks. This ratio is an indication of the extent of superimposed noise. Table II presents the ratios of the second to the first nearest neighbor spacing (A_1 for second peak/ A_1 for first peak) and those of the third to the first nearest neighbor spacing (A_1 for third peak/ A_1 for first peak) for all the samples examined in this study.

C. Frequency Distribution of Coordination Number for Cells and Dendrites

Figure 5 shows the frequency distribution of the coordination number (number of nearest neighbors) for cells and



(a)



(b)

Fig. 2—Typical microstructures of directionally solidified Pb-2.2 wt pct Sb alloy (thermal gradient $G_L = 86 \text{ K/cm}$): (a) dendritic growth at $V = 18.4 \mu\text{m/s}$ and (b) cellular growth at $V = 1.5 \mu\text{m/s}$.

dendrites as observed on the transverse sections of the directionally solidified Pb-2.2 wt pct Sb alloy samples. It includes data from seven different growth speeds at the temperature gradient of 86 K cm^{-1} . Growth speeds less than $1.8 \mu\text{m s}^{-1}$ correspond to the cells and growth speeds larger than $1.8 \mu\text{m s}^{-1}$ to the dendrites. There is considerable scatter in the data. However, six nearest neighbors appear to be predominant. This becomes more evident if we combine all the data, irrespective of their growth speeds, into one overall frequency distribution. Such overall frequency distributions

for the thermal gradients of 40 K cm^{-1} (seven growth speeds), 86 K cm^{-1} (11 growth speeds), and 140 K cm^{-1} (seven growth speeds) are presented in Figure 6. Now, the overwhelming dominance of six as the coordination number is clearly evident.

Cells and dendrites both show the predominance of six as their coordination number, as indicated in Figure 7, which contains data for the Pb-2.2 wt pct Sb alloy. Figure 7(a) combines all the frequency distributions for dendrites, irrespective of the growth speeds and thermal gradients, and

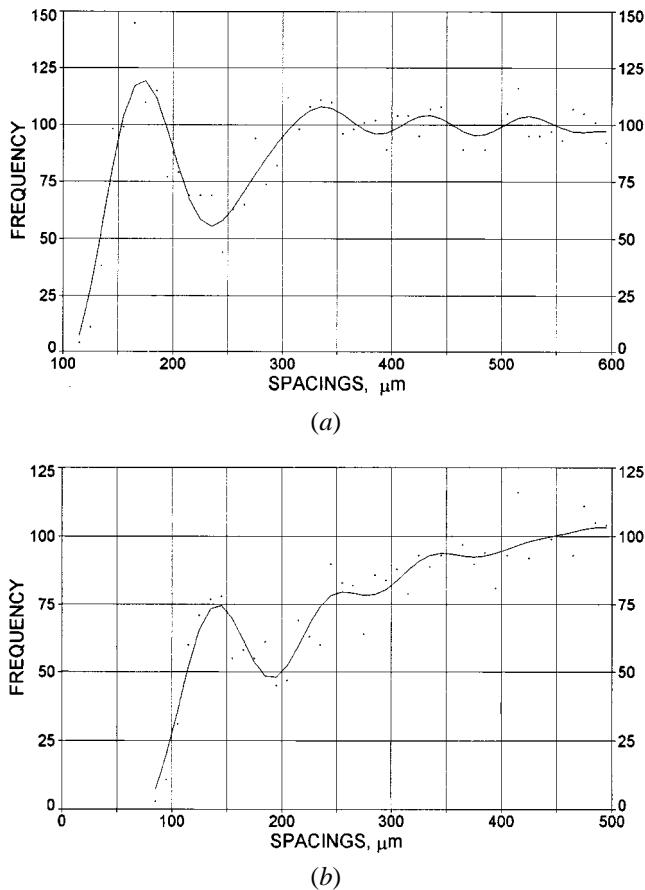


Fig. 3—Typical distribution of nearest and higher-order neighbor spacing (thermal gradient $G_L = 86$ K/cm): (a) dendritic growth at $V = 18.4 \mu\text{m/s}$ and (b) cellular growth at $V = 1.5 \mu\text{m/s}$.

Figure 7(b) does the same for the cells. The lines through the data represent Gaussian regression. The regression parameters are presented in Table III. The r^2 values are nearly unity, indicating an excellent fit to the Gaussian behavior. The parameter A_1 is 6.46 ± 0.05 for dendrites, and 6.13 ± 0.06 for cells.

The influence of thermosolutal convection in the mushy zone on the distribution of cells and dendrites can be observed by comparing Figures 7 and 8, which correspond to Pb-2.2 wt pct Sb and Pb-5.8 wt pct Sb, respectively. Comparison of the Gaussian regression parameters in Table III shows that the higher extent of convection in the mushy zone expected in the more permeable PB-5.8 wt pct Sb alloy does not cause any significant change in the statistical distribution of cells and dendrites.

IV. DISCUSSION

The data presented in Table II show the ratio of the second to the first neighbor spacing (A_2/A_1 for second peak/ A_1 for first peak) to be 1.85 ± 0.11 and that of the third to the first neighbor spacing (A_3/A_1 for third peak/ A_1 for first peak) to be 2.70 ± 0.25 . For an ideal square distribution of the cells and dendrites, these ratios would be 1.414 and 2, respectively. For an ideal hexagonal distribution, the ratios would be 1.73 and 2.2, respectively. Assuming that we have more confidence in the experimentally observed ratio between

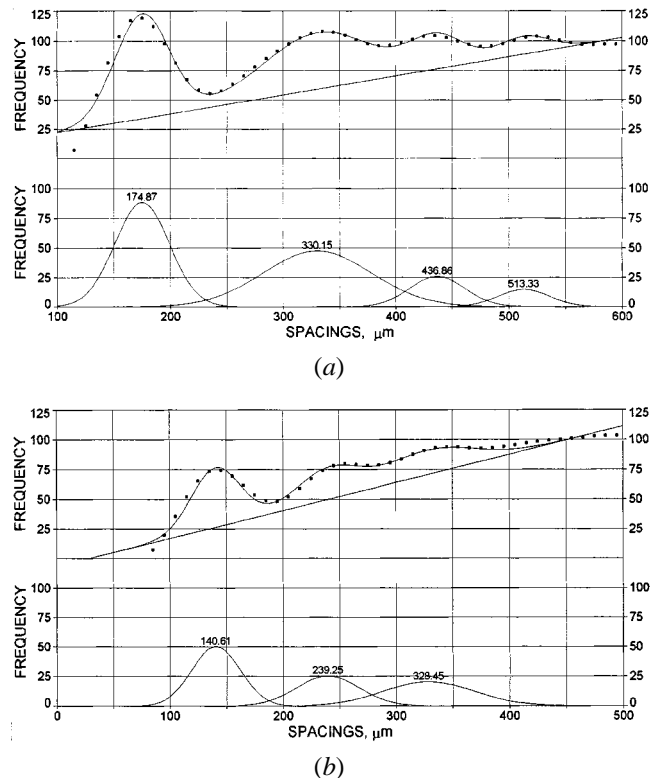


Fig. 4—Gausse amplitude fit to the spacing distribution (thermal gradient $G_L = 86$ K/cm): (a) dendritic growth at $V = 18.4 \mu\text{m/s}$ and (b) cellular growth at $V = 1.5 \mu\text{m/s}$.

the second and the first nearest neighbor spacing, 1.85, the experimental observations are closer to that for the hexagonal arrangement (1.73) than to a square one (1.4). This is also supported by the observed frequency distributions of the coordination number of the cells and dendrites (Figures 5 through 8). Combining all the cell and dendrite data presented in Table III, we obtain $A_1 = 6.3$, suggesting the predominance of a hexagonal arrangement. The mean value of the ratio A_2/A_1 is 0.13 for Gaussian regression of the frequency distribution (Table III), and is 0.214 for Gaussian regression of the nearest neighbor peak (Table I). This, however, indicates that there is considerable Gaussian noise superimposed on this hexagonal arrangement of the cells and dendrites.

There are three sources of noise: fluctuations in the growth speed and thermal gradient caused by mechanical effects, variation in grain orientations across the specimen cross section, and fluid flow due to convection. In addition, there may be a scatter inherent in the primary spacing distribution, as indicated by the recently reported history dependence of primary spacing.^[13] In this study, growth speed and thermal gradient are well controlled, and grain orientations are well aligned (Figure 2). Convection in the mushy zone is known to produce nonuniform distribution of cells and dendrites. In a more severe form, it can produce “channel segregates” or “freckles.”^[12] We believe that convection is the major contributor of this noise, as has been indicated by preliminary low-gravity experiments that produced more uniform microstructure.^[14] However, the question remains of what extent of this noise is caused by convection in the melt, and what extent of it is inherent in the arrayed growth of the cells and dendrites? Only convection-free low-gravity directional

Table I. Spacings in Directionally Solidified Pb-2.2 Wt Pct Sb Alloy (Thermal Gradient $G_L = 86 \text{ K cm}^{-1}$)

Velocity ($\mu\text{m s}^{-1}$)	First Peak				Second Peak			Third Peak			r^2
	A_0	A_1	A_2	A_1/A_2	A_0	A_1	A_2	A_0	A_1	A_2	
1.5	21.3	140.6	79.8	0.568	28.0	239.3	76.8	40.5	328.5	52.4	0.960
2.1	42.8	235.0	33.2	0.141	24.5	455.1	46.6	1.2	642.3	47.1	0.963
2.5	19.0	197.1	28.5	0.145	21.6	365.5	39.4	20.3	523.4	22.4	0.994
3	29.0	205.7	43.0	0.21	26.7	355.1	47.8	29.3	515.1	73.2	0.988
6	19.8	205.2	35.9	0.175	12.8	384.9	40.6	4.7	515.9	48.7	0.992
10	86.0	179.8	28.6	0.159	81.5	345.2	47.2	88.5	525.2	13.9	0.982
14	53.9	194.1	33.6	0.173	54.5	357.1	43.7	42.3	453.1	23.3	0.994
18.2	88.1	174.9	24.3	0.139	47	330.1	48.5	25.8	436.9	24.6	0.98
mean = 0.214											

Table II. The Ratios of the Second to the First Nearest Neighbor Spacings and of the Third to the First Nearest Neighbor Spacings in Directionally Solidified Pb-Sb Alloys

Velocity ($\mu\text{m s}^{-1}$)	Solute Content (Wt Pct Sb)	Thermal Gradient (K cm^{-1})	Morphology	Peak 2/Peak 1	Peak 3/Peak 1	r^2
1.5	2.2	86	cell	1.70	2.90	0.96
2.1	2.2	86	cell/dendrite	1.94	2.73	0.963
2.5	2.2	86	dendrite	1.85	2.65	0.994
3.0	2.2	86	dendrite	1.73	2.50	0.988
6.0	2.2	86	dendrite	1.88	2.51	0.992
10	2.2	86	dendrite	1.91	2.89	0.982
14	2.2	86	dendrite	1.92	2.33	0.994
18.2	2.2	86	dendrite	1.83	2.69	0.911
0.6	2.2	37	cell	1.98	2.91	0.984
10	2.2	37	dendrite	1.48	2.07	0.978
0.8	5.8	140	cell	1.93	2.75	0.995
1.0	5.8	140	cell	1.86	2.60	0.875
1.5	5.8	140	early dendrite	1.83	2.41	0.930
2.0	5.8	140	early dendrite	1.89	3.05	0.992
3.0	5.8	140	dendrite	1.94	2.97	0.990
3.5	5.8	140	dendrite	1.80	2.74	0.997
8.0	5.8	140	dendrite	1.82	2.68	0.994
10	5.8	140	dendrite	1.89	2.99	0.993
20	5.8	140	dendrite	1.91	2.87	0.973
				mean = 1.85	mean = 2.70	
				standard deviation = ± 0.11	standard deviation = ± 0.25	

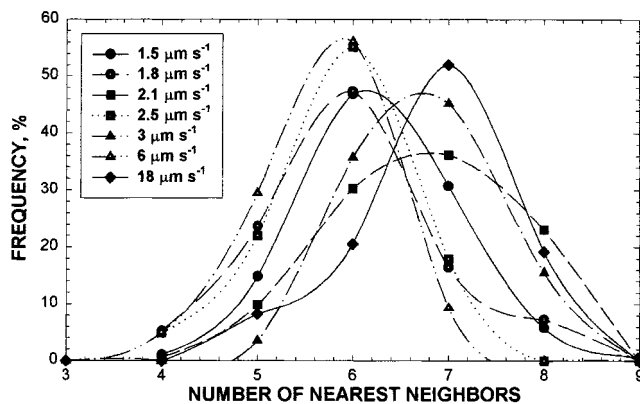


Fig. 5—Frequency distribution of number of nearest neighbors in a directionally solidified Pb-2.2 wt pct Sb alloy (thermal gradient $G_L = 86 \text{ K cm}^{-1}$).

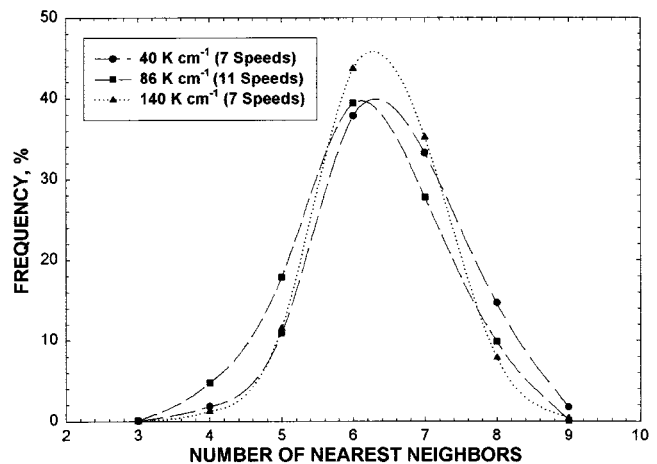


Fig. 6—Combined frequency distribution of number of nearest neighbors in a directionally solidified Pb-2.2 wt pct Sb alloy under three different thermal gradients.

solidification experiments on single crystal samples and their comparison with the terrestrial experiments would provide an answer. Such experiments are presently planned.

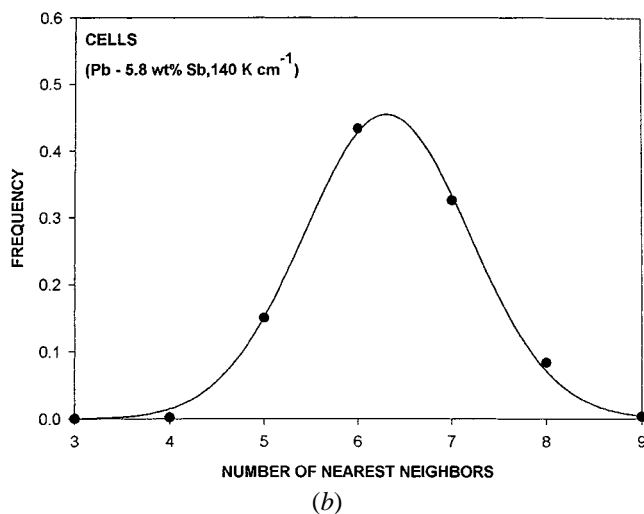
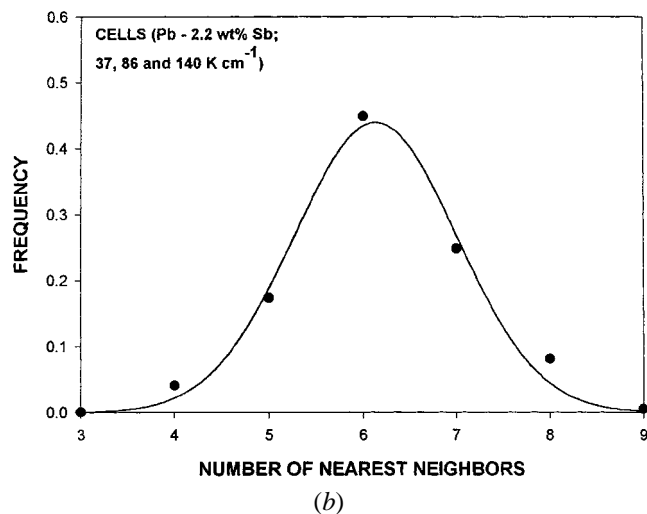
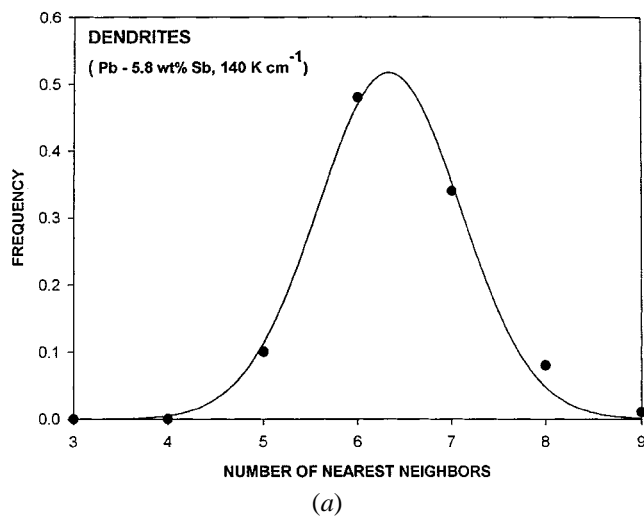
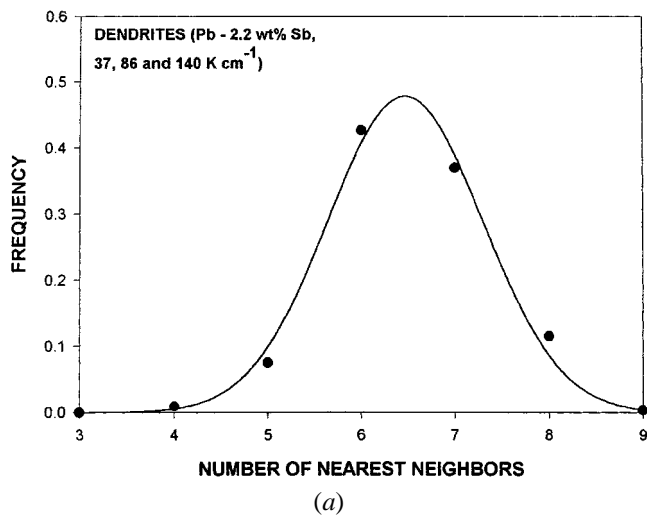


Fig. 7—Frequency distribution of number of nearest neighbors in a directionally solidified Pb-2.2 wt pct Sb alloy irrespective of growth speeds or thermal gradients for (a) dendrites and (b) cells.

Fig. 8—Frequency distribution of number of nearest neighbors in a directionally solidified Pb-5.8 wt pct Sb alloy irrespective of growth speeds at $G = 140 \text{ K cm}^{-1}$ for (a) dendrites and (b) cells.

Table III. Gaussian Regression of the Frequency Distribution of the Number of Nearest Neighbors in Directionally Solidified Pb-Sb Alloys

Solute Content (Wt Pct Sb)	Morphology	A_0	A_1	A_2	r^2	A_2/A_1
2.2	dendrite	0.48 ± 0.03	6.46 ± 0.05	0.83 ± 0.05	0.99	0.13
2.2	cell	0.44 ± 0.03	6.13 ± 0.06	0.87 ± 0.06	0.98	0.14
5.8	dendrite	0.52 ± 0.02	6.33 ± 0.04	0.76 ± 0.04	0.99	0.12
5.8	cell	0.46 ± 0.01	6.31 ± 0.02	0.88 ± 0.02	0.99	0.14

V. CONCLUSIONS

The following conclusions can be drawn from the statistical analysis of the cell/dendrite distribution on the transverse sections of the directionally solidified Pb-2.2 wt pct Sb and Pb-5.8 wt pct Sb alloy samples.

- (1) The cells and dendrites both have an inherent hexagonal distribution.
- (2) There is considerable Gaussian noise superimposed on

this hexagonal distribution. Convection in the mushy zone may be partially responsible for this noise.

ACKNOWLEDGMENTS

This research was supported by the Microgravity Materials Research Program at NASA-Marshall Space Flight Center (Huntsville, AL). Appreciation is expressed to Professors

Rohit Trivedi and David Poirier for many helpful discussions.

REFERENCES

1. J.D. Hunt and S.Z. Lu: *Metall. Mater. Trans. A*, 1996, vol. 27A, pp. 611-23.
2. J.A. Warren and J.S. Langer: *Phys. Rev. E.*, 1993, vol. E47, pp. 2702-12.
3. B.J. Braun and B.T. Murray: *J. Cryst. Growth*, 1997, vol. 174, pp. 41-53.
4. A. Karma and W.J. Rappel: *J. Cryst. Growth*, 1997, vol. 174, pp. 54-64.
5. M.S. Bhat, D.R. Poirier, J.C. Heinrich, and D. Nagelhout: *Scripta Metall. Mater.*, 1994, vol. 31, pp. 339-44.
6. B.J. Spencer and H.E. Huppert: *Acta Mater.*, 1998, vol. 46, pp. 2645-62.
7. B. Billia, H. Jamgotchian, and H. Nguyen Thi: *Metall. Trans. A*, 1991, vol. 22A, pp. 3041-50.
8. W.D. Huang, X.G. Geng, and Y.H. Zhou: *J. Cryst. Growth*, 1993, vol. 134, pp. 105-15.
9. S.H. Han and R. Trivedi: *Acta Mater.*, 1994, vol. 42, pp. 25-34.
10. M.H. Burden, D.J. Hebditch, and J.D. Hunt: *J. Cryst. Growth*, 1973, vol. 20, pp. 121-24.
11. M.A. Chopra and S.N. Tewari: *Metall. Trans. A*, 1991, vol. 22A, pp. 2467-74.
12. J.R. Sazarin and A. Hellawell: *Metall. Trans. A*, 1988, vol. 19A, pp. 1861-71.
13. W.D. Huang, X.G. Geng, and Y.H. Zhou: *J. Cryst. Growth*, 1993, vol. 134, pp. 105-16.
14. J.J. Favier, J. Berthier, P. Arragon, and Y. Malmejac: *Acta Astronautica*, 1982, vol. 9, pp. 255-59.